JPE 17-1-15

https://doi.org/10.6113/JPE.2017.17.1.149
ISSN(Print): 1598-2092 / ISSN(Online): 2093-4718

An Adaptive Speed Estimation Method Based on a Strong Tracking Extended Kalman Filter with a Least-Square Algorithm for Induction Motors

Zhonggang Yin†, Guoyin Li*, Chao Du*, Xiangdong Sun*, Jing Liu*, and Yanru Zhong*

†,*Department of Electrical Engineering, Xi'an University of Technology, Xi'an, China

Abstract

To improve the performance of sensorless induction motor (IM) drives, an adaptive speed estimation method based on a strong tracking extended Kalman filter with a least-square algorithm (LS-STEKF) for induction motors is proposed in this paper. With this method, a fading factor is introduced into the covariance matrix of the predicted state, which forces the innovation sequence orthogonal to each other and tunes the gain matrix online. In addition, the estimation error is adjusted adaptively and the mutational state is tracked fast. Simultaneously, the fading factor can be continuously self-tuned with the least-square algorithm according to the innovation sequence. The application of the least-square algorithm guarantees that the information in the innovation sequence is extracted as much as possible and as quickly as possible. Therefore, the proposed method improves the model adaptability in terms of actual systems and environmental variations, and reduces the speed estimation error. The correctness and the effectiveness of the proposed method are verified by experimental results.

Key words: Adaptive speed estimation, Fading factor, Induction Motor (IM), Least-Square (LS) algorithm, Strong Tracking Extended Kalman Filter (STEKF)

NOMENCLATURE

α, β	Stationary reference frame axes.
d, q	Rotary reference frame axes.
a, b, c	Three-phase reference frame axes.
$i_{s\alpha}$, $i_{s\beta}$	α-Axis and β-Axis stator currents, A.
i_{sd}, i_{sq}	d-Axis and q-Axis stator currents, A.
i_a, i_b, i_c	a-Axis, b-Axis and c-Axis stator currents, A.
$u_{s\alpha}$, $u_{s\beta}$	α-Axis and β-Axis stator voltages, V.
u_{sd}, u_{sq}	d-Axis and q-Axis stator voltages, V.
$\psi_{r\alpha}$, $\psi_{r\beta}$	α-Axis and β-Axis rotor flux linkages, Wb.
V_{dc}	DC link voltage, V.
$\square^*$	Reference quantity.
J	Moment of inertia.
θ	Rotor position.
ω_{sl}	Slip frequency, rad/s.
ω_r	Angular rotor speed, rad/s.
L_m	Mutual inductance, H.
$L_{s\sigma}$	Stator leakage inductance, H.
$L_{r\sigma}$	Rotor leakage inductance, H.
L_s, L_r	Stator and rotor inductances, H.
σ	(=1-(L_m^2/L_sL_r)) Total leakage coefficient.
σ_r	Rotor leakage coefficient.
σ_s	Stator leakage coefficient.
R_s, R_r	Stator and rotor resistances, Ω.
T_r	(=L_r/R_r) Rotor time constant.
T	Sampling period, μs.
$\boldsymbol{v}_k$	System noise.
$\boldsymbol{w}_k$	Measurement noise.
T_L	Rated torque, N·m.
P	Pole pair.
P_N	Rated power, kW.
U_N	Rated voltage, V.
I_N	Rated current, A.
f_N	Rated frequency, Hz.

Manuscript received May 6, 2016; accepted Sep. 12, 2016
Recommended for publication by Associate Editor Dong-Hee Lee.
†Corresponding Author: zhgyin@xaut.edu.cn
Tel: +86-029-86312650, Xi'an University of Technology
*Dept. of Electrical Engineering, Xi'an University of Technology, China

I. INTRODUCTION

Induction motors (IM) have many advantageous characteristics, such as high robustness, reliability and low cost compared with DC motors. The installation of speed

sensors increases the cost, and reduces the robustness and the reliability of induction motor (IM) drives. Therefore, a lot of attention has been paid to rotor speed estimation to achieve sensorless control. Many sensorless methods have been proposed, such as high-frequency signal injection [1], [2], model reference adaptive systems (MRAS) [3], [4], full-order adaptive observers [5]–[7], sliding-mode observers (SMO) [8], [9], artificial neural networks (ANN) [10], and extended Kalman filters (EKF) [11]–[29].

References [1] and [2] use a method to estimate speed based on high-frequency signal injection, and they obtain good performance. The speed sensorless control methods based on signal injection are capable of long-term stability at zero stator frequency. However, they are highly sophisticated and require customized designs for a particular motor drive, and there are estimated speed delays to the rotor speed due to the filter. Reference [3] presents a closed-loop model reference adaptive system (CL-MRAS), and a speed observer is developed for linear induction motor (LIM) drives. A new formulation of the reactive-power-based MRAS that is stable in all four quadrants of operation is proposed in [4]. However, in these studies, with respect to sensorless IM drives, the rotor flux and load torque should be known to realize the sensorless controller. Moreover, these observers usually lose effectiveness or give inaccurate results due to the fact that they lack observability at low speeds. In [5], [6] and [7], new design rules for the adaptation of PI gains to satisfy the required performances are proposed. The robustness of the adaptive full-order observer against stator resistance and inductance variations is also investigated. However, the speed fluctuations becomes large as the speed decreases. In [8] and [9], a SMO is used to estimate speed and to identify the stator resistance and overcome the problems of stator resistance variations, particularly for low-speed operation. However, since the scheme is designed based on a mathematical model of an IM, its observability is generally lost at zero magnetic field frequency, and the SMO experiences chattering. In [11], a new method based on ANNs applied to the parameter estimation of induction motors using sensorless vector control is proposed. Results obtained with this observer are more efficient than the results obtained with the classical observer.

Unlike the other methods, the EKF takes a stochastic approach to state estimation. In spite of its computational complexity, the EKF makes on-line state estimation possible while simultaneously performing the identification of parameters in a relatively short time interval, while taking the system and measurement noises directly into account. Recently, the EKF has been studied widely in terms of the speed sensorless control of motors. In [11] and [12], an EKF is used for speed and flux linkage estimation in direct torque control systems. Experimental results show that the systems based on the EKF have good performance and applicable value. In [13] and [14], an EKF is used as a speed and position estimator in the vector control system of PMSMs. The control bandwidth is enhanced and the identification problems due to the low-order state equations of IPMSMs can be avoided, and the estimation error of the rotor position based on the identified permanent magnet flux is limited to within a very low level. In [15] and [16], the torque and position are estimated by an EKF in a stepper motor. This method can cancel the static error and compensate load torque variations. In addition, good position estimation can be achieved. Because of the massive calculation with a five-order matrix, most of the research results are only verified by simulations. In order to apply it to practice, a reduced-order EKF algorithm for flux and speed estimation is proposed in [17] and [18], and the speed and flux linkage are estimated easily. In [19], an EKF has been used to estimate the rotor speed, rotor flux, stator flux and stator currents accurately in the vector control systems of the induction motors, and a small stator current THD is confirmed. Depending on the commanded speed, either the rotor current model or the open-loop stator voltage model is proposed for an EKF to achieve better performance in a wide speed range, including the field-weakening region. Reference [20] presents a novel sensorless stator-flux-oriented sliding-mode scheme based on an offline optimized-delayed state Kalman filter algorithm to estimate the stator-flux components and the rotor speed in IMs, and it obtains good performance. In [21], the application of optimal state estimation and optimal state feedback algorithms based on an EKF for real-time active magnetic bearing control is treated. It is shown that the controller yields more accurate rotor position estimation, better system dynamics, higher bearing stiffness, and reduced control energy effort compared with the conventionally used proportional-integral-differential control approaches. In [22] and [23], a parameter estimator based on an EKF is used to estimate the rotor resistance and mutual inductance. The results motivate the utilization of the proposed estimation technique in combination with a variety of control methods for IMs.

However, the extended Kalman filter is poorly robust against model uncertainties, which results in inaccuracy in terms of EKF state estimations when the model mismatches, and it can even cause the system to diverge [24]. When the system reaches the stable state, the Kalman gain and the error covariance matrix are limited to within a low level, and the tracking ability to the mutations is lost. The EKF cannot track these changes quickly when the external environment is mutated. The main contribution of this paper is that an adaptive speed estimation method for induction motors based on a strong tracking EKF with the least-square algorithm (LS-STEKF) is proposed to improve model adaptability to actual systems and environment variations, and to reduce the speed estimation error. With this method, the fading factor is

introduced into the covariance matrix of the predicted state, which force the innovation sequence orthogonal to each other and tunes the gain matrix online. In addition, the estimation error is adjusted adaptively and the mutational state is tracked quickly. Simultaneously, the proposed method tunes the fading factor by extracting information from the innovation sequence as much as possible with the least-square algorithm. The correctness and effectiveness of the proposed method are verified by experimental results.

II. EKF OBSERVER FOR INDUCTION MOTORS

The mathematical model of an induction motor can be described by the following equations:

$$\frac{di_{s\alpha}}{dt}=(-\frac{R_s}{\sigma L_s}+\frac{1-\sigma}{\sigma T_r})i_{s\alpha}+\frac{L_m}{\sigma L_s L_r T_r}\psi_{r\alpha}+\omega_r\frac{L_m}{\sigma L_s L_r}\psi_{r\beta}+\frac{1}{\sigma L_s}u_{s\alpha} \quad (1)$$

$$\frac{di_{s\beta}}{dt}=(-\frac{R_s}{\sigma L_s}+\frac{1-\sigma}{\sigma T_r})i_{s\beta}-\omega_r\frac{L_m}{\sigma L_s L_r}\psi_{r\alpha}+\frac{L_m}{\sigma L_s L_r T_r}\psi_{r\beta}+\frac{1}{\sigma L_s}u_{s\beta} \quad (2)$$

$$\frac{d\psi_{r\alpha}}{dt}=\frac{L_m}{T_r}i_{s\alpha}-\frac{1}{T_r}\psi_{r\alpha}-\omega_r\psi_{r\beta} \quad (3)$$

$$\frac{d\psi_{r\beta}}{dt}=\frac{L_m}{T_r}i_{s\beta}-\frac{1}{T_r}\psi_{r\beta}+\omega_r\psi_{r\alpha} \quad (4)$$

$$\frac{d\omega_r}{dt}=\frac{p^2L_m}{JL_r}(i_{s\beta}\psi_{r\alpha}-i_{s\alpha}\psi_{r\beta})-\frac{p}{J}T_L \quad (5)$$

$$\boldsymbol{Y}=\begin{bmatrix} i_{s\alpha} & i_{s\beta}\end{bmatrix}^T \quad (6)$$

Models (1)-(6) are nonlinear and multivariable, and they are affected by parametric uncertainties. Moreover, the load torque T_L is unknown. For speed estimation, an approach is based on the assumption that speed varies slowly with respect to electromagnetic variables. It is suggested that $\dot{\omega}_r=0$ should be substituted in (5) to obtain a fifth-order model.

The mathematical models of an induction motor are described by (1)-(6) when ω_r is known. However, ω_r is unknown in sensorless control, and the resulting model is nonlinear.

The system equation and observer equation are supposed to be linear for Kalman filters. However, the actual system cannot satisfy this supposition. Nonlinear systems can approximate linear systems with EKFs, and the calculation precision is enhanced with this algorithm. The EKF is formulated as follows:

$$\frac{d\hat{\boldsymbol{x}}}{dt}=\boldsymbol{A}\hat{\boldsymbol{x}}+\boldsymbol{B}\boldsymbol{u}+\boldsymbol{K}(\boldsymbol{y}-\hat{\boldsymbol{y}}) \quad (7)$$

$$\hat{\boldsymbol{y}}=\boldsymbol{H}\hat{\boldsymbol{x}} \quad (8)$$

where $\hat{\boldsymbol{x}}$ is the state variable, $\hat{\boldsymbol{y}}$ is the observation variable, $\boldsymbol{u}$ is the control variable, $\boldsymbol{y}$ is the actual measurement value, $\boldsymbol{A}$ is the state matrix, $\boldsymbol{B}$ is the input matrix, $\boldsymbol{H}$ is the observation matrix, and $\boldsymbol{K}$ is the gain matrix.

For the EKF, some unmeasured variables can be calculated from the measured value. Generally, the stator voltage and stator current are set to be the measured vector, namely $\boldsymbol{u}=\boldsymbol{u}_s$, $\boldsymbol{y}=\boldsymbol{i}_s$.

From models (7) and (8), the EKF is explained using the following nonlinear time-invariant state model:

$$\hat{\boldsymbol{x}}_k=\boldsymbol{A}_k\hat{\boldsymbol{x}}_{k-1}+\boldsymbol{B}_k\boldsymbol{u}_k+\boldsymbol{K}_k(\boldsymbol{y}-\hat{\boldsymbol{y}}) \quad (9)$$

$$\hat{\boldsymbol{y}}_k=\boldsymbol{H}_k\hat{\boldsymbol{x}}_k \quad (10)$$

where $\boldsymbol{A}_k$, $\boldsymbol{B}_k$, and $\boldsymbol{H}_k$ are the discretized matrixes of $\boldsymbol{A}$, $\boldsymbol{B}$, and $\boldsymbol{H}$, respectively. $\tilde{\bullet}$ is the prediction, and $\hat{\bullet}$ is the updated value.

$$\boldsymbol{x}_k=(i_{s\alpha,k}\quad i_{s\beta,k}\quad \psi_{r\alpha,k}\quad \psi_{r\beta,k}\quad \omega_{r,k})^T,$$

$$\boldsymbol{u}_k=(u_{s\alpha,k}\quad u_{s\beta,k})^T,$$

$$\boldsymbol{A}_k=\begin{bmatrix} 1-\frac{T}{T'_{sr}} & 0 & \frac{TL_m}{\sigma L_s L_r T_r} & \hat{\omega}_r\frac{TL_m}{\sigma L_s L_r} & 0\\ 0 & 1-\frac{T}{T'_{sr}} & -\hat{\omega}_r\frac{TL_m}{\sigma L_s L_r} & \frac{TL_m}{\sigma L_s L_r T_r} & 0\\ \frac{TL_m}{T_r} & 0 & 1-\frac{T}{T_r} & -T\hat{\omega}_r & 0\\ 0 & \frac{TL_m}{T_r} & T\hat{\omega}_r & 1-\frac{T}{T_r} & 0\\ 0 & 0 & 0 & 0 & 1\end{bmatrix}$$

$$,\boldsymbol{B}_k=\begin{bmatrix}\frac{T}{\sigma L_s} & 0\\ 0 & \frac{T}{\sigma L_s}\\ 0 & 0\\ 0 & 0\\ 0 & 0\end{bmatrix},\quad \boldsymbol{H}_k=\begin{bmatrix}1 & 0 & 0 & 0 & 0\\ 0 & 1 & 0 & 0 & 0\end{bmatrix},$$

$T'_{sr}=\sigma L_s/R_{sr}$, $R_{sr}=R_s+(L_m/L_r)^2R_r$, $T_r=L_r/R_r$.

T is the sampling period, and a suitable distance of the sampling period to the system electric constant is kept. $\boldsymbol{v}_k$ is the system noise, and $\boldsymbol{w}_k$ is the measured noise.

$$\mathrm{cov}(\boldsymbol{v}_k,\boldsymbol{v}_i)=E\{\boldsymbol{v}_k\boldsymbol{v}_i^T\}=\begin{cases}\boldsymbol{Q}, i=k\\ 0, i\neq k\end{cases} \quad (11)$$

$$\mathrm{cov}(\boldsymbol{w}_k,\boldsymbol{w}_i)=E\{\boldsymbol{w}_k\boldsymbol{w}_i^T\}=\begin{cases}\boldsymbol{R}, i=k\\ 0, i\neq k\end{cases} \quad (12)$$

$$\mathrm{cov}(\boldsymbol{w}_k,\boldsymbol{v}_i)=E\{\boldsymbol{w}_k\boldsymbol{v}_i^T\}=0,\ \text{for all } i \text{ and } k \quad (13)$$

Both vector $\boldsymbol{w}_k$ and vector $\boldsymbol{v}_k$ are zero-mean Gaussian white sequences with a zero cross correlation with each other, and $\boldsymbol{Q}$ and $\boldsymbol{R}$ are positive definite matrices. The covariance matrix of the system noise $\boldsymbol{Q}$ accounts for the model inaccuracy, the system disturbances, and the noise introduced by voltage measurements (sensor noise and A/D converter quantization). The covariance matrix of the measurement noise $\boldsymbol{R}$ accounts for the measurement noise introduced by the current sensors

and A/D quantization.

In many cases, saturation is taken into account. It is assumed that saturation leads to a decrease in the mutual inductance L_m. Consequently, saturation affects the values of the rotor and stator inductances given by:

$$L_r = L_{r\sigma} + L_m \tag{14}$$

$$L_s = L_{s\sigma} + L_m \tag{15}$$

In the EKF, deviation is used to feedback correction, and the specific process includes following steps:

1) Prediction of the state variable:

$$\tilde{\boldsymbol{x}}_k = \boldsymbol{A}_k \hat{\boldsymbol{x}}_{k-1} + \boldsymbol{B}_k \boldsymbol{u}_k \tag{16}$$

2) Prediction of the error covariance matrix $\tilde{\boldsymbol{P}}_k$:

$$\tilde{\boldsymbol{P}}_k = \boldsymbol{G}_k \hat{\boldsymbol{P}}_{k-1} \boldsymbol{G}_k^T + \boldsymbol{Q}_k \tag{17}$$

where $\boldsymbol{G}_k = \left(\frac{\partial}{\partial x}(\boldsymbol{A}_k \boldsymbol{x} + \boldsymbol{B}_k \boldsymbol{u}_k)\right)\Big|_{\boldsymbol{x}=\tilde{\boldsymbol{x}}_k}$

$$= \begin{bmatrix} 1-\frac{T}{T'_{sr}} & 0 & \frac{TL_m}{\sigma L_s L_r T_r} & \tilde{\omega}_{r,k}\frac{TL_m}{\sigma L_s L_r} & \frac{TL_m}{\sigma L_s L_r}\tilde{\psi}_{r\beta,k} \\ 0 & -\frac{T}{T'_{sr}} & -\tilde{\omega}_{r,k}\frac{TL_m}{\sigma L_s L_r} & \frac{TL_m}{\sigma L_s L_r T_r} & -\frac{TL_m}{\sigma L_s L_r}\tilde{\psi}_{r\alpha,k} \\ \frac{TL_m}{T_r} & 0 & 1-\frac{T}{T_r} & -T\tilde{\omega}_{r,k} & -T\tilde{\psi}_{r\beta,k} \\ 0 & \frac{TL_m}{T_r} & T\tilde{\omega}_{r,k} & 1-\frac{T}{T_r} & T\tilde{\psi}_{r\alpha,k} \\ 0 & 0 & 0 & 0 & 1 \end{bmatrix}$$

3) Calculation of the Kalman filter gain matrix:

$$\boldsymbol{K}_k = \tilde{\boldsymbol{P}}_k \boldsymbol{H}_k^T (\boldsymbol{H}_k \tilde{\boldsymbol{P}}_k \boldsymbol{H}_k^T + \boldsymbol{R}_k)^{-1} \tag{18}$$

4) Update of the state prediction variable:

$$\hat{\boldsymbol{x}}_k = \tilde{\boldsymbol{x}}_k + \boldsymbol{K}_k (\boldsymbol{y}_k - \boldsymbol{H}_k \tilde{\boldsymbol{x}}_k) \tag{19}$$

5) Update of the error covariance matrix $\hat{\boldsymbol{P}}_k$:

$$\hat{\boldsymbol{P}}_k = (\boldsymbol{I} - \boldsymbol{K}_k \boldsymbol{H}_k)\tilde{\boldsymbol{P}}_k \tag{20}$$

III. STEKF Observer with the Least-Square Algorithm

In the EKF, a nonlinear system can be approximated by a linear system and the basic form of a linear Kalman equations is kept. Because the Kalman gain can adapt to the environment for adjustments, the EKF has some adaptive ability. However, the EKF is poorly robust against model uncertainties, which results in inaccuracy of EKF state estimations, and can even cause the system to diverge. When the system reaches a stable state, the Kalman gain and the error covariance matrix are limited to within a small value, and the tracking ability to the mutations is lost. The EKF cannot track these changes quickly when the external environment is mutated. An adaptive speed estimation method based on a strong tracking EKF with the least-square algorithm (LS-STEKF) for induction motors is proposed to solve the above problems. With this method, the fading factor is introduced into the covariance matrix of the predicted state, which forces the innovation sequence orthogonal to each other and tunes the gain matrix online. The estimation error is adjusted adaptively, and the mutational state is tracked quickly. Simultaneously, the proposed method searches for the fading factor with the least-square algorithm, which makes the information in the innovation sequence extract as much as possible and as quickly as possible. The proposed method shows more robustness against the model uncertainties or time-varying parameter systems, and it has better tracking ability in the presence of mutations and slow changes. Therefore, the proposed method improves the model adapt to actual systems and environmental variations, and reduces the speed estimation error. A block diagram of the speed estimation based on the STEKF is shown in Fig. 1.

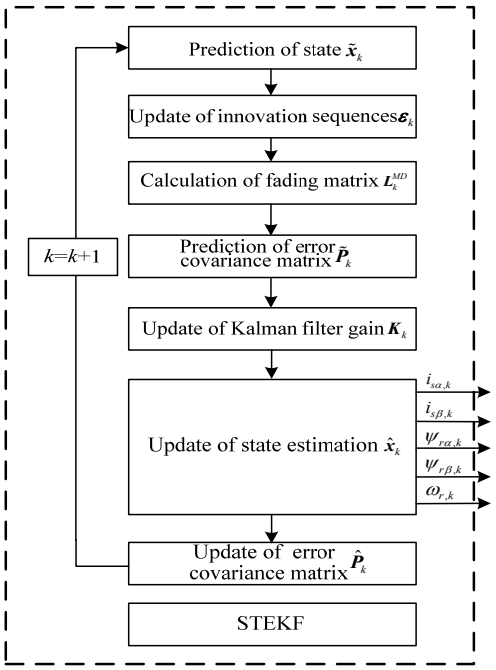

Fig. 1. Block diagram of speed estimation based on STEKF.

A. STEKF for Rotor Speed Estimation

The state estimation issue which the strong tracking EKF solves is described as follows:

$$\boldsymbol{x}_k = f(\boldsymbol{x}_{k-1}) + \boldsymbol{\Gamma}_k \boldsymbol{v}_k \tag{21}$$

$$\boldsymbol{y}_k = \boldsymbol{H}_k x_k + \boldsymbol{w}_k \tag{22}$$

The innovation sequence between the measured value and the predicted value is as follows:

$$\boldsymbol{\varepsilon}_k = \boldsymbol{y}_k - \tilde{\boldsymbol{y}}_k \tag{23}$$

The strong tracking EKF meets following orthogonal principle:

$$\boldsymbol{E}([\boldsymbol{x}_k - \hat{\boldsymbol{x}}_k][\boldsymbol{x}_k - \hat{\boldsymbol{x}}_k]^T) = \min \tag{24}$$

$$\boldsymbol{E}(\boldsymbol{\varepsilon}_k \boldsymbol{\varepsilon}_k^T) = 0 \tag{25}$$

Equation (24) and (25) are required for ensuring that the innovation sequence remains orthogonal. The fading factor is incorporated for the online tuning of the covariance matrix of the predicted state, which adjusts the filter gain, and accordingly the STEKF is developed. The fading matrix can be expressed as follows:

$$\boldsymbol{L}_k^{MD} = diag[\gamma_k^1, \gamma_k^2, \cdots, \gamma_k^n] \tag{26}$$

Compared with the EKF, the prediction error covariance matrix of the STEKF becomes as follows:

$$\tilde{\boldsymbol{P}}_k = \boldsymbol{L}_k^{MD} \boldsymbol{G}_k \hat{\boldsymbol{P}}_{k-1} \boldsymbol{G}_k^T + \boldsymbol{Q}_k \tag{27}$$

$$\gamma_k^i = \begin{cases} \beta_i c_k, & \beta_i c_k > 1 \\ 1, & \beta_i c_k \le 1 \end{cases} \tag{28}$$

$$c_k = tr[\boldsymbol{N}_k] / tr[\boldsymbol{M}_k] \tag{29}$$

where $tr[]$ is the trace of the matrix.

$$\boldsymbol{N}_k = \boldsymbol{V}_k - \boldsymbol{R}_k - \boldsymbol{H}_k \boldsymbol{Q}_k \boldsymbol{H}_k^T \tag{30}$$

$$\boldsymbol{M}_k = \boldsymbol{H}_k \boldsymbol{G}_k \hat{\boldsymbol{P}}_{k-1} \boldsymbol{G}_k^T \boldsymbol{H}_k^T \tag{31}$$

$$\boldsymbol{V}_k = \begin{cases} \boldsymbol{\varepsilon}_1 \boldsymbol{\varepsilon}_1^T, & k = 1 \\ \dfrac{\rho \boldsymbol{V}_{k-1} + \boldsymbol{\varepsilon}_k \boldsymbol{\varepsilon}_k^T}{1+\rho}, & k \ge 2 \end{cases} \tag{32}$$

β_i is a constant determined by prior information, where $\beta_i \ge 1$. c_k is the undetermined factor. ρ is the forgetting factor, where $0 \le \rho \le 1$. A forgetting factor of 0.95 is commonly used in the STEKF. The modeling error can be reduced by adjusting γ_k in a timely manner to obtain almost the same mean tracking errors for the STEKF, which is also indicated by other studies.

The fading factor γ_k in the STEKF method increases the accuracy of the state estimation model, according to the extent determined by the information in the innovation sequence. When fast environmental variations and parameter variations produce $\gamma_k > 1$ due to the magnitude innovations, the STEKF provides an appropriate factor γ_k to improve the adaptive ability to the actual systems, subsequently yielding an accurate speed estimation. When the system under normal conditions yields $\gamma_k = 1$ owing to the accuracy of the state estimation model, the STEKF becomes the standard EKF, and yields an accurate speed estimation.

B. Analysis of Seeking Mechanism for the Fading Factor

It can be seen from (29) that:

$$tr[\boldsymbol{N}_k] = tr[\boldsymbol{V}_k] - tr[\boldsymbol{R}_k - \boldsymbol{H}_k \boldsymbol{Q}_k \boldsymbol{H}_k^T] \tag{33}$$

In (33), $tr[\boldsymbol{R}_k - \boldsymbol{H}_k \boldsymbol{Q}_k \boldsymbol{H}_k^T]$ is not affected by $\boldsymbol{\varepsilon}_k$, and it is assumed that:

$$tr[\boldsymbol{R}_k - \boldsymbol{H}_k \boldsymbol{Q}_k \boldsymbol{H}_k^T] = \boldsymbol{\delta}_k \tag{34}$$

Equation (33) can be rewritten as follows:

$$tr[\boldsymbol{N}_k] = tr[\boldsymbol{V}_k] - \boldsymbol{\delta}_k = \frac{\rho}{1+\rho} tr[\boldsymbol{V}_{k-1}] + \frac{1}{1+\rho}[(\boldsymbol{\varepsilon}_k^1)^2 + (\boldsymbol{\varepsilon}_k^2)^2 + \cdots + (\boldsymbol{\varepsilon}_k^m)^2] - \boldsymbol{\delta}_k \tag{35}$$

From (29) and (35), the denominator is not affected by $\boldsymbol{\varepsilon}_k$, and c_k only depends on $\boldsymbol{\varepsilon}_k$. The magnitude of the output $\boldsymbol{y}_k$ is relatively large in the actual practice. However, the estimated results are directly affected by $\boldsymbol{\varepsilon}_k$, and the absolute value of the residuals is very different when the relative residuals are equal, which results in residual information asymmetry. Therefore, the estimation precision and response speed are reduced. This is due to the fact that the traditional suboptimal algorithm is applied to reduce the calculating work online when searching for the fading factor, and the algorithm only extracts information of the diagonal elements in $\boldsymbol{M}_k$ and $\boldsymbol{N}_k$, and ignores the other information. In order to improve the estimation precision and the response speed, the proposed method searches for the fading factor in the STEKF with the least-square algorithm.

C. Parameter Identification Principles of the Least-Square Algorithm

The system equations can be expressed as:

$$\boldsymbol{z}_k = \boldsymbol{h}_k \boldsymbol{\Phi}_k = \tilde{\boldsymbol{z}}_k + \boldsymbol{d}_k = \tilde{\boldsymbol{h}}_k \boldsymbol{\Phi}_k + \boldsymbol{d}_k \tag{36}$$

where $\boldsymbol{z}_k$ is the output, $\tilde{\boldsymbol{h}}_k$ is the estimated state vector, $\boldsymbol{\Phi}_k$ is the observation matrix, and $\boldsymbol{d}_k$ is the estimation error.

$$\boldsymbol{d}_k = \begin{bmatrix} e_k(1) & e_k(2) & \cdots & e_k(n) \end{bmatrix} \tag{37}$$

According to the least-square principle, $\tilde{\boldsymbol{h}}_k$ is the least-square estimation value when the quadratic sum of the error is minimal.

$$S = \sum_{i=1}^{n} e_k{}^2(i) = \min \tag{38}$$

The quadratic sum of the error, which the estimated parameter vector $\tilde{\boldsymbol{h}}_k$ satisfies (38), is as follows:

$$\begin{aligned} S = \sum_{i=1}^{n} e_k{}^2(i) = \boldsymbol{d}_k^T \boldsymbol{d}_k = \tilde{\boldsymbol{h}}_k^T \boldsymbol{\Phi}_k^T \boldsymbol{\Phi}_k \tilde{\boldsymbol{h}}_k + \\ \boldsymbol{z}_k^T \boldsymbol{z}_k - \boldsymbol{z}_k^T \boldsymbol{\Phi} \tilde{\boldsymbol{h}}_k - \tilde{\boldsymbol{h}}_k^T \boldsymbol{\Phi}_k^T \boldsymbol{z}_k \end{aligned} \tag{39}$$

Equation (39) can be organized as follows:

$$\begin{aligned} S = \left[\boldsymbol{\Phi}_k^T \boldsymbol{\Phi}_k \tilde{\boldsymbol{h}}_k - \boldsymbol{\Phi}_k^T \boldsymbol{z}_k \right]^T (\boldsymbol{\Phi}_k^T \boldsymbol{\Phi}_k)^{-1} \left[\boldsymbol{\Phi}_k^T \boldsymbol{\Phi}_k \tilde{\boldsymbol{h}}_k - \boldsymbol{\Phi}_k^T \boldsymbol{z}_k \right] + \\ \left[\boldsymbol{z}_k^T \boldsymbol{z}_k - \boldsymbol{z}_k^T \boldsymbol{\Phi} (\boldsymbol{\Phi}_k^T \boldsymbol{\Phi}_k)^{-1} \boldsymbol{\Phi}_k^T \boldsymbol{z}_k \right] \end{aligned} \tag{40}$$

From (40), S consists of two parts:

part 1: $\left[\boldsymbol{\Phi}_k^T \boldsymbol{\Phi}_k \tilde{\boldsymbol{h}}_k - \boldsymbol{\Phi}_k^T \boldsymbol{z}_k \right]^T (\boldsymbol{\Phi}_k^T \boldsymbol{\Phi}_k)^{-1} \left[\boldsymbol{\Phi}_k^T \boldsymbol{\Phi}_k \tilde{\boldsymbol{h}}_k - \boldsymbol{\Phi}_k^T \boldsymbol{z}_k \right]$

part 2: $\left[\boldsymbol{z}_k^T \boldsymbol{z}_k - \boldsymbol{z}_k^T \boldsymbol{\Phi} (\boldsymbol{\Phi}_k^T \boldsymbol{\Phi}_k)^{-1} \boldsymbol{\Phi}_k^T \boldsymbol{z}_k \right]$

Part 1 is positive, and part 2 has no correlation with $\tilde{\boldsymbol{h}}_k$. Therefore, in order to make S minimum, part 1 has to be zero. Thus:

$$\boldsymbol{\Phi}_k^T \boldsymbol{\Phi}_k \tilde{\boldsymbol{h}}_k - \boldsymbol{\Phi}_k^T \boldsymbol{z}_k = 0 \tag{41}$$

The estimated value is obtained by:

$$\tilde{\boldsymbol{h}}_k = (\boldsymbol{\Phi}_k^T \boldsymbol{\Phi}_k)^{-1} \boldsymbol{\Phi}_k^T \boldsymbol{z}_k \tag{42}$$

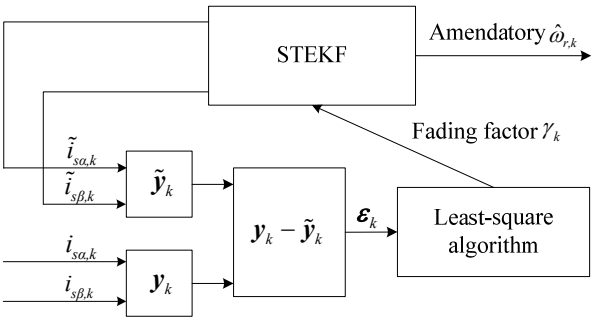

Fig. 2. Speed estimation structure based on LS-STEKF.

D. STEKF with the Least-Square Algorithm to Tune the Fading Factor

According to the above analysis, an adaptive approach with the least-square algorithm is used to tune the fading factor, and the structure of the LS-STEKF is shown in Fig. 2.

The theory innovation variance should match the real-time identification variance. Thus:

$$\boldsymbol{H}_k \boldsymbol{L}_k^{MD} \boldsymbol{G}_k \hat{\boldsymbol{P}}_{k-1} \boldsymbol{G}_k^T \boldsymbol{H}_k^T = \boldsymbol{V}_k - \boldsymbol{R}_k - \boldsymbol{H}_k \boldsymbol{Q}_k \boldsymbol{H}_k^T \tag{43}$$

$$\boldsymbol{L}_k^{MD} = c_k diag\left[\beta_1, \beta_2, \cdots \beta_n\right] \tag{44}$$

$$\boldsymbol{N}_k = c_k \boldsymbol{\alpha}_k \tag{45}$$

where:

$$\boldsymbol{\alpha}_k = \boldsymbol{H}_k \boldsymbol{\beta} \boldsymbol{G}_k \hat{\boldsymbol{P}}_{k-1} \boldsymbol{G}_k^T \boldsymbol{H}_k^T \tag{46}$$

$$\boldsymbol{\beta} = diag\left[\beta_1, \beta_2, \cdots \beta_n\right] \tag{47}$$

According to $\boldsymbol{\alpha}_k$ and $\boldsymbol{N}_k$, the vectors can be structured as follows:

$$\boldsymbol{\Psi}_k = \begin{bmatrix} \boldsymbol{N}_k[1,1] \\ \cdots \\ \boldsymbol{N}_k[1,m] \\ \cdots \\ \boldsymbol{N}_k[m,1] \\ \cdots \\ \boldsymbol{N}_k[m,m] \end{bmatrix} \tag{48} \qquad \boldsymbol{\Xi}_k = \begin{bmatrix} \boldsymbol{\alpha}_k[1,1] \\ \cdots \\ \boldsymbol{\alpha}_k[1,m] \\ \cdots \\ \boldsymbol{\alpha}_k[m,1] \\ \cdots \\ \boldsymbol{\alpha}_k[m,m] \end{bmatrix} \tag{49}$$

By least-square algorithm, c_k is given by:

$$c_k = \left(\boldsymbol{\Xi}_k^T \boldsymbol{\Xi}_k\right)^{-1} \boldsymbol{\Xi}_k^T \boldsymbol{\Psi}_k = \frac{\sum_{i,j=1}^{m} \boldsymbol{\alpha}_k[i,j] \boldsymbol{N}_k[i,j]}{\sum_{i,j=1}^{m} \boldsymbol{\alpha}_k^2[i,j]} \tag{50}$$

Only the diagonal elements of $\boldsymbol{M}_k$ and $\boldsymbol{N}_k$ are used in (29). However, all of the elements are used based on the least-square algorithm, which means that more information is used to tune the fading factor, and c_k, optimized by least-square algorithm, is used to tune the fading factor γ_k.

It is the essence of the sensorless vector control that the motor speed is not acquired by a mechanical sensor, but rather by software in a speed regulating system. A block diagram of the sensorless vector control system for induction motors is shown in Fig. 3.

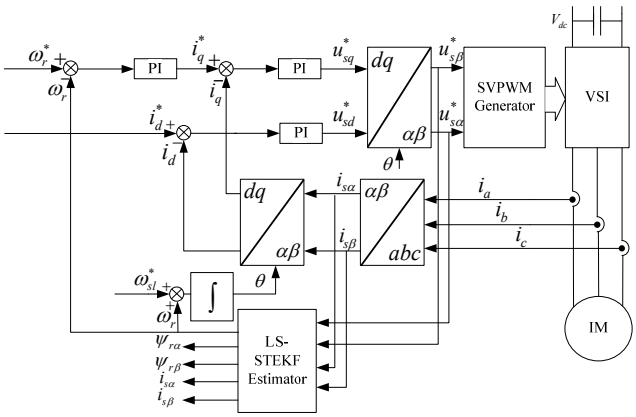

Fig. 3. Block frame of sensorless vector control based on LS-STEKF.

The voltage and phase current of the induction motor are transformed to the α-β coordinate system. The voltage and current based in the α-β coordinate system are the inputs of the LS-STEKF estimator. The rotor speed is estimated and fed back to the PI controller. The control voltages ($u_{s\alpha}$*, $u_{s\beta}$*) are transformed to u_{sd} and u_{sq}, which are the outputs of the PI controller. At last, the outputs of the SVPWM are loaded into a PWM inverter to regulate the induction motor. The outputs are the speed, current and flux based on the α-β coordinate system.

IV. EXPERIMENTAL RESULTS

In order to validate the performance of the estimator, the above speed estimation methods are implemented on a control platform based on a TMS320F28335. The parameters of the induction motor are shown in TABLE I, and the experimental platform is shown in Fig. 4. The system hardware consists of an induction motor, an IM inverter, a loading system, and an oscilloscope. The loading system includes a loading servo motor and a servo inverter. The induction motor is driven by the inverter. The stator voltage, stator current and rotor speed are measured by a Hall effect voltage sensor, a Hall effect current sensor and a photoelectric coder, respectively.

The system software process includes the initialization, main loop, fault protection, PWM interrupt, etc. The period of the PWM interrupt is 125 μs, and the main functions include the coordinate transformation, LS-STEKF algorithm, dead time compensation, SVPWM generation, etc.

The covariance matrices $\boldsymbol{Q}$ and $\boldsymbol{R}$ are taken to be diagonal. If a large value of the matrix $\boldsymbol{R}$ is used, the transient response decreases but the state is well estimated in the steady state. As shown in (18), the matrices K and R are inversely

TABLE I
MOTOR PARAMETERS

P_N	1.1 kW	R_s	5.27 Ω
U_N	380 V	R_r	5.07 Ω
I_N	2.7 A	L_m	0.421 H
f_N	50 Hz	L_s	0.423 H
T_L	7.5 N·m	L_r	0.479 H
J	0.02 kg·m^2	σL_s	0.053 H
n_N	1410 r/min	P	2

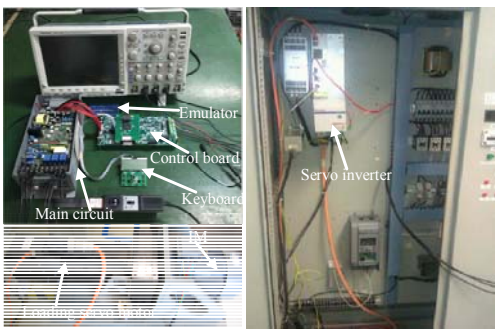

Fig. 4. Experimental platform.

proportional. Therefore, the value of $\boldsymbol{K}$ becomes weak in order to give more accuracy to the estimation of the state. Otherwise, the overshoot in the transient response and the noises in the steady-state response are obtained. In both cases, $\boldsymbol{R}$ acts on the transient response and the steady-state response because its value is constant in the EKE algorithm. The covariance matrix $\boldsymbol{Q}$ represents the noises on the system due to the modeling errors. From (17) and (18), the matrix $\boldsymbol{K}$ is proportional to the matrix $\boldsymbol{Q}$. Then, it has the opposite effect of that of $\boldsymbol{R}$. Under the premise to ensure convergence, the choice of every values for these matrices is done according to the dynamics of the state variables and the performance index. The value of the $\boldsymbol{Q}$ and $\boldsymbol{R}$ matrices for the EKF and the LS-STEKF are $\boldsymbol{R} = diag[0.1, 0.1]$, $\boldsymbol{Q} = diag[2\times10^{-2}, 2\times10^{-2}, 2\times10^{-3}, 2\times10^{-3}, 1]$.

A. Experimental Verification for Speed Estimation during Full Speed and Low Speed

When the motor runs at different speeds, experimental results based on the LS-STEKF are shown in Fig. 5. The estimated speed and the speed estimation error are given from top to bottom. It can be seen that the motor runs at six stages, including 30 r/min, 300 r/min, 900 r/min, 1500 r/min, 1200 r/min and 600 r/min, respectively, which contain the full range of running speeds. This indicates that the proposed method has good tracking performance.

Fig. 6 shows the estimated speed response based on the LS-STEKF at a step speed from +15 r/min to +150 r/min. The step reference speed, the estimated speed, and the speed estimation error are given from top to bottom. This shows

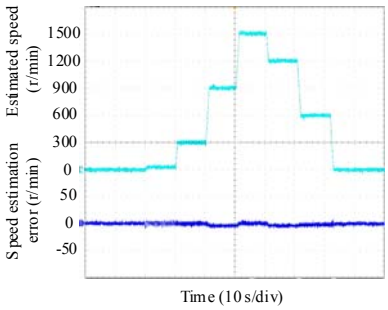

Fig. 5. Speed tracking performance in whole operation based on LS-STEKF.

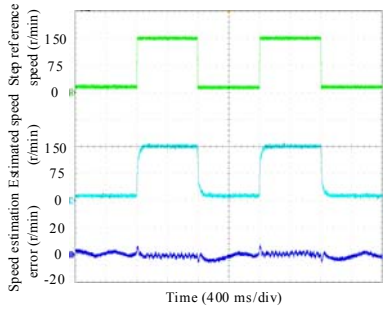

Fig. 6. Speed tracking performance at step speed from +15 r/min to +150 r/min.

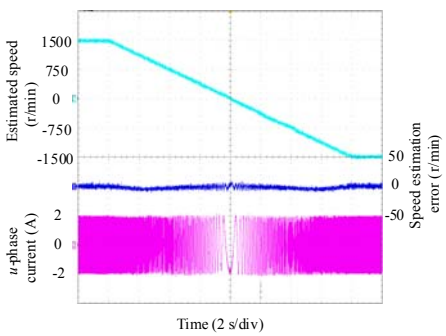

Fig. 7. Estimated speed and stator current at switching point of reversal.

that the LS-STEKF can quickly respond to step reference speed changes, and has good tracking performance in the low speed range.

Fig. 7 shows the estimated speed and stator current based on the LS-STEKF when the given speed ranges from +1500 r/min to -1500 r/min. The estimated speed, the speed estimation error, and the *u*-phase current are given from top to bottom. This indicates that in the process of the motor speed reversal, the current waveform has no oscillation or transition. In addition, the estimated speed based on the LS-STEKF remains stable, and smooth switching is achieved on the zero-crossing position.

Fig. 8 shows the estimated speed and the stator current based on the LS-STEKF at 9 r/min. The estimated speed, the speed estimation error, and the *u*-phase current are given from top to bottom. It can be seen that the stator current is

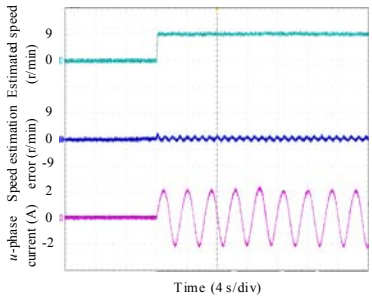

Fig. 8. Estimated speed and stator current at 9 r/min.

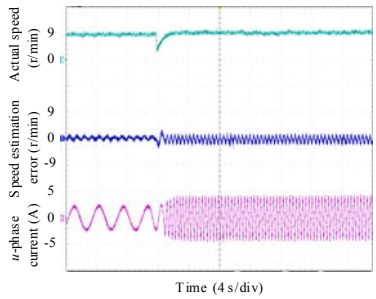

Fig. 9. Experimental results based on LS-STEKF at 9 r/min with step load from 0 to 100% rated torque.

close to sine, and that the motor can operate stably at low speeds.

Fig. 9 shows experimental results based on the LS-STEKF at 9 r/min with a step load from 0 to 100% of the rated torque. The rotor speed, the speed estimation error, and the *u*-phase current are given from top to bottom. It can be seen that the motor speed can track the given speed again very soon after the load changes rapidly, and that the motor can run stably at low speeds with 100% of the rated load. Therefore, the LS-STEKF has good dynamic performance against step loads at low speeds.

Figs. 5-9 demonstrate the correctness of the speed estimation system based on LS-STEKF.

B. Robustness to Motor Parameter Mismatches

Fig. 10 shows the estimated speed and the speed estimation error of the EKF and the LS-STEKF at 30 r/min with $1.3R_s$. The estimated speed and the speed estimation error are given from top to bottom. Fig. 10(a) shows experimental results based on the EKF, and Fig. 10(b) shows experimental results based on the LS-STEKF. As shown in Fig. 10, the estimated speed based on the EKF has a larger fluctuation than that of the LS-STEKF with a mismatched R_s. At the same time, the maximum error of the speed estimation is reduced to 4 r/min from 8 r/min based on the LS-STEKF when R_s mismatches.

Fig. 11 shows the estimated speed and speed estimation error of the EKF and the LS-STEKF at 30 r/min with $0.7R_s$. The estimated speed and the speed estimation error are given from top to bottom. Fig. 11(a) shows the experimental results based on the EKF, and Fig. 11(b) shows the experimental results based on the LS-STEKF. From the experimental

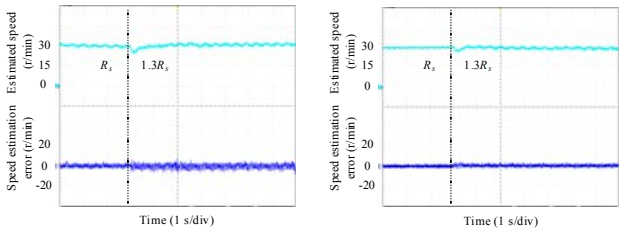

(a) (b)

Fig. 10. Experimental comparison of the estimated speed and the speed estimation error at 30 r/min with $1.3R_s$. (a) EKF. (b) LS-STEKF.

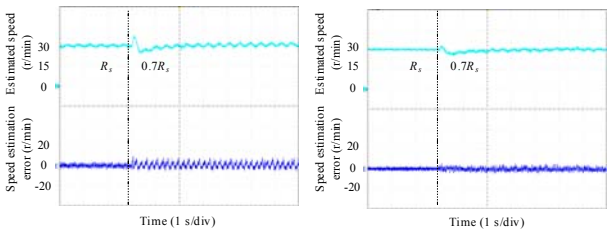

(a) (b)

Fig. 11. Experimental comparison of the estimated speed and the speed estimation error at 30 r/min with $0.7R_s$. (a) EKF. (b) LS-STEKF.

results, it can be seen that the estimated speed based on the EKF has a large fluctuation with a mismatched R_s, and that the maximum error of the speed estimation is 10 r/min. However, the speed estimation fluctuation based on the LS-STEKF is rather small, and the maximum error of the speed estimation is reduced to 5 r/min.

Fig. 12 shows the estimated speed and speed estimation error of the EKF and the LS-STEKF at 30 r/min with $1.3L_m$. The estimated speed and the speed estimation error are given from top to bottom. Fig. 12(a) shows the experimental results based on the EKF, and Fig. 12(b) shows the experimental results based on the LS-STEKF. It can be seen that the estimated speed based on the EKF has a larger fluctuation than that of the LS-STEKF with a mismatched L_m. In addition, the maximum error of the speed estimation is reduced to 3 r/min from 7 r/min based on the LS-STEKF.

Fig. 13 shows the estimated speed and speed estimation error of the EKF and the LS-STEKF at 30 r/min with $0.7L_m$. The estimated speed and the speed estimation error are given from top to bottom. Fig.13(a) shows the experimental results based on the EKF, and Fig. 13(b) shows the experimental results based on the LS-STEKF. It can be seen that the estimated speed based on the EKF has a large fluctuation with a mismatched L_m. In addition, the maximum speed estimation error is 8 r/min. However, the speed estimation fluctuation of the LS-STEKF is rather small, and the maximum error of the speed estimation is reduced to 4 r/min.

Figs. 10-13 indicate that the EKF is more sensitive to motor parameter mismatches, and that the LS-STEKF has better robustness to motor parameter mismatches.

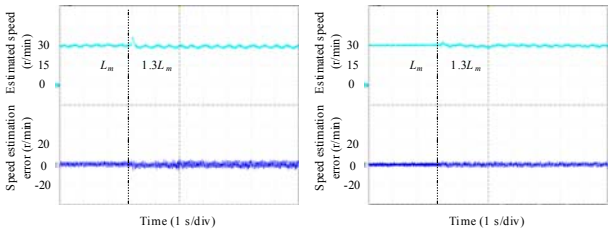

(a) (b)

Fig. 12. Experimental comparison of the estimated speed and the speed estimation error at 30 r/min with 1.3L_m. (a) EKF. (b) LS-STEKF.

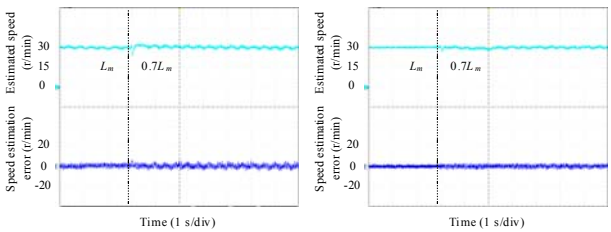

(a) (b)

Fig. 13. Experimental comparison of the estimated speed and the speed estimation error at 30 r/min with 0.7L_m. (a) EKF. (b) LS-STEKF.

C. With a Gross Estimation Error

Fig. 14 shows the estimated speed and speed estimation error of the EKF and the LS-STEKF when an error vector which is $[1\ 0\ 0\ 0\ 0]^T$ is added to $\boldsymbol{x}$, and the given speed is 1500 r/min. The estimated speed and the speed estimation error are given from top to bottom. Fig. 14(a) shows the experimental results based on the EKF, and Fig. 14(b) shows the experimental results based on the LS-STEKF. It can be seen that the maximum fluctuation of the estimated speed and the maximum error of the speed estimation are obviously reduced when a gross estimation error occurs. The maximum fluctuation of the estimated speed is reduced to 25 r/min from 125 r/min, and the maximum error of the speed estimation is reduced to 20 r/min from 50 r/min. Therefore, the LS-STEKF has better anti-estimation-error capability than the EKF.

D. With a Gross External Disturbance

In order to test the anti-error capability of the LS-STEKF, a disturbance pulse valued at 2 A is added to the current detection channels by a signal generator when the given speed is 1500 r/min. Fig. 15 shows the estimated speed and the speed estimation error of the EKF and the LS-STEKF. The estimated speed and the speed estimation error are given from top to bottom. Fig. 15(a) shows the experimental results based on the EKF, and Fig. 15(b) shows the experimental results based on the LS-STEKF. From the experimental results, it can be seen that the maximum fluctuation of the estimated speed is reduced to 30 r/min from 135 r/min, and that the maximum error of the speed estimation is reduced to 25 r/min from 60 r/min. Therefore, the LS-STEKF has better anti-error capability than the EKF.

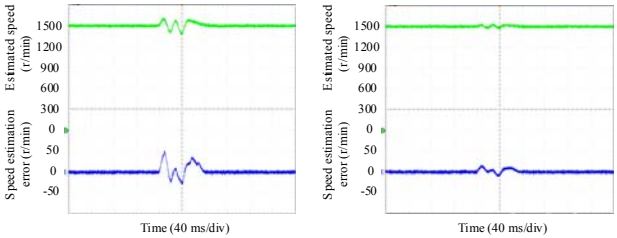

(a) (b)

Fig. 14. Experimental comparison of the estimated speed and the speed estimation error at 1500 r/min with gross estimation error. (a) EKF. (b) LS-STEKF.

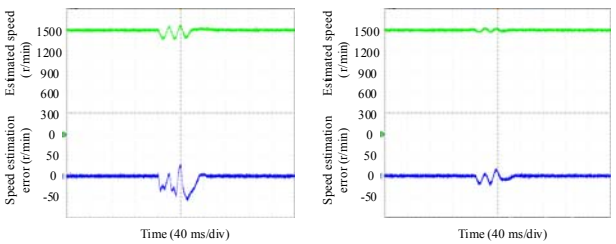

(a) (b)

Fig. 15. Experimental comparison of the estimated speed and the speed estimation error at 1500 r/min with gross external disturbance. (a) EKF. (b) LS-STEKF.

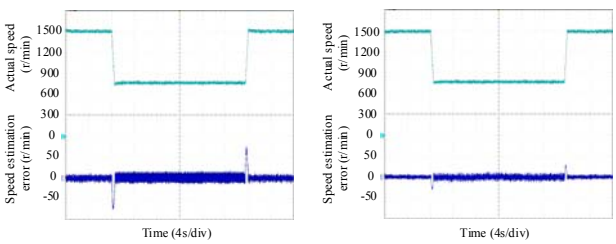

(a) (b)

Fig. 16. Experimental comparison of the speed estimation error with the speed slew rate of 1500 r/min/s at deceleration and acceleration under 80% rated load. (a) EKF. (b) LS-STEKF.

E. Dynamic Performance Verification at Fast and Slow Speed Slew Rates with a Load

Fig. 16 shows a speed estimation error comparison with the EKF and the LS-STEKF at fast speed deceleration and acceleration with a 80% rated load, and a speed slew rate of 1500 r/min/s. The rotor speed and the speed estimation error are given from top to bottom. Fig. 16(a) shows the experimental results based on the EKF, and Fig. 16(b) shows the experimental results based on the LS-STEKF. It can be seen that the maximum speed estimation error is obviously reduced based on the LS-STEKF at a speed slew rate of 1500 r/min/s, and the maximum error of the speed estimation is reduced to 30 r/min from 75 r/min.

Fig. 17 shows a speed estimation error comparison with the EKF and the LS-STEKF at slow speed acceleration and deceleration with an 80% rated load, and a speed slew rate of 200 r/min/s. The rotor speed and the speed estimation error

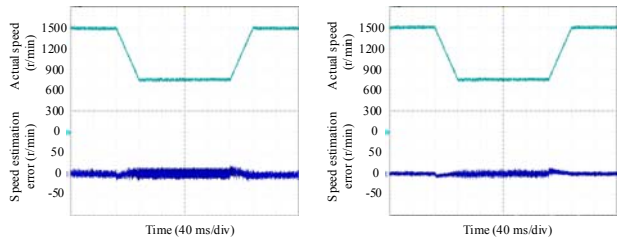

(a) (b)

Fig. 17. Experimental comparison of the speed estimation error with the speed slew rate of 200 r/min/s at deceleration and acceleration under 80% rated load. (a) EKF. (b) LS-STEKF.

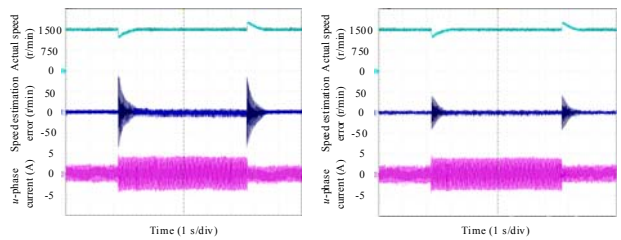

(a) (b)

Fig. 18. Experimental comparison of the speed estimation error at 1500 r/min with step load disturbance from 0 to 100% rated torque. (a) EKF. (b) LS-STEKF.

are given from top to bottom. Fig. 17(a) shows the experimental results based on the EKF, and Fig. 17(b) shows the experimental results based on the LS-STEKF. The motor decelerates from 1500 r/min to 750 r/min and then accelerates to 1500 r/min. From the experimental results, the maximum error of the speed estimation is reduced to 12 r/min from 25 r/min with the LS-STEKF during the whole speed deceleration and acceleration.

Fig. 16 and Fig. 17 show that the superiority of the LS-STEKF is that it has better dynamic performance than the EKF at both fast and slow speed slew rates with a load.

F. Dynamic Performance Verification with a Step Load

Fig. 18 shows a speed estimation error comparison with the EKF and the LS-STEKF at 1500 r/min with a step load disturbance from 0 to 100% of the rated torque. The rotor speed, the speed estimation error, and the *u*-phase current are given from top to bottom. Fig. 18(a) shows the experimental results based on the EKF, and Fig. 18(b) shows the experimental results based on the LS-STEKF. It can be seen that the speed estimation error is obviously reduced based on the LS-STEKF during the entire operation with the step load disturbance, and that the maximum error of the speed estimation is reduced to 40 r/min from 90 r/min. Therefore, the LS-STEKF is effective for sensorless control and has better dynamic tracking performance than the EKF at high speeds with a step load.

Fig. 19 shows a speed estimation error comparison with the EKF and the LS-STEKF at 150 r/min with a step load disturbance from 0 to 100% of the rated torque. The rotor speed, the speed estimation error, and the *u*-phase current are

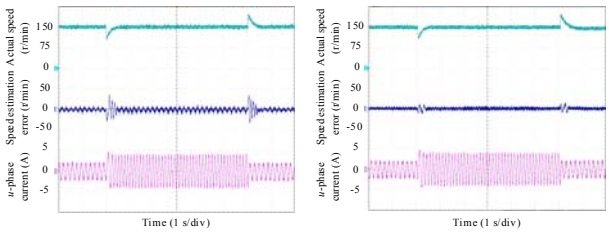

(a) (b)

Fig. 19. Experimental comparison of the speed estimation error at 150 r/min with step load disturbance from 0 to 100% rated torque. (a) EKF. (b) LS-STEKF.

given from top to bottom. Fig. 19(a) shows the experimental results based on the EKF, and Fig. 19(b) shows the experimental results based on the LS-STEKF. It can be seen that the speed estimation error is obviously reduced based on the LS-STEKF during the entire operation with the step load disturbance, and that the maximum error of the speed estimation is reduced to 10 r/min from 35 r/min. Therefore, the LS-STEKF is effective for sensorless control and has better dynamic tracking performance than the EKF at low speeds with a step load.

Fig. 18 and Fig. 19 indicate that the superiority of LS-STEKF is that it has better dynamic performance than the EKF with a step load disturbance.

V. CONCLUSION

In this paper, an adaptive speed estimation method based on the LS-STEKF for induction motors has been proposed. The correctness and effectiveness of the proposed method have been verified on an induction motor sensorless drive. Experimental results demonstrate that the LS-STEKF can effectively improve the model adaptability to actual systems and environmental variations. The maximum error of the speed estimation with disturbances and motor parameter mismatches is obviously reduced, and both the steady and transient performances are improved by using the proposed adaptive speed estimation method.

ACKNOWLEDGMENT

The authors would like to acknowledge the financial support of National Natural Science Foundation of China (51677150, 51307139), Specialized Research Fund of Shaanxi Province (2015KJXX-29), and Industrial Research Projects of Shaanxi Province (2014K06-29).

REFERENCES

[1] C. Caruana, G. M. Asher, and M. Sumner, "Performance of HF signal injection techniques for zero-low-frequency vector control of induction machines under sensorless conditions," *IEEE Trans. Ind. Electron.*, Vol. 53, No. 1, pp. 225-238, Feb. 2006.

[2] L. Y. Xu, E. Inoa, Y. Liu, and B. Guan, "A new high-frequency injection method for sensorless control of doubly fed induction machines," *IEEE Trans. Ind. Appl.*, Vol. 48, No. 5, pp. 1556-1564, Sep/Oct. 2012.

[3] A. Accetta, M. Cirrincione, M. Pucci, and G. Vitale, "Closed-loop MRAS speed observer for linear inductionmotor drives," *IEEE Trans. Ind. Appl.*, Vol.51, No.3, pp. 2279-2290, May/Jun. 2015.

[4] T. Orlowska-Kowalska and M. Dybkowski, "A new formulation of reactive-power-based model reference adaptive system for sensorless induction motor drive," *IEEE Trans. Ind. Electron.*, Vol. 62, No. 11, pp. 6797-6807, Nov. 2015.

[5] M. S. Zaky, "Stability analysis of speed and stator resistance estimators for sensorless induction motor drives," *IEEE Trans. Ind. Electron.*, Vol. 59, No. 2, pp. 858-870, Feb. 2012.

[6] W. Sun, Y. Yu, G. L. Wang, B. B. L, and D. G. Xu "Design method of adaptive full order observer with or without estimated flux error in speed estimation algorithm," *IEEE Trans. Power. Electron.*, Vol. 31, No. 3, pp. 2609-2626, Mar. 2016.

[7] S. Po-ngam and S. Sangwongwanich, "Stability and dynamic performance improvement of adaptive full-order observers for sensorless PMSM drive," *IEEE Trans. Power Electron.*, Vol. 27, No. 2, pp. 588-600, Feb. 2012.

[8] R. P. Vieira, C. C. Gastaldini, R. Z. Azzolin, and H. A. Gründling, "Sensorless sliding-mode rotor speed observer of induction machines based on magnetizing current estimation," *IEEE Trans. Ind. Electron.*, Vol. 61, No. 9, pp. 4573-4582, Sep. 2014.

[9] L. H. Zhao, J. Huang, B. N. Li, and W. B. Kong, "Second-order sliding-mode observer with online parameter identification for sensorless induction motodrives," *IEEE Trans. Ind. Electron.*, Vol. 61, No. 10, pp. 5280-5289, Oct. 2014.

[10] X. D. Sun, L. Chen, Z. B. Yang, and H. Q. Zhu, "Speed-sensorless vector control of a bearingless induction motor with artificial neural network inverse speed observer." *IEEE Trans. on Mechatron*., Vol. 18, No. 4, pp. 1357-1366, Aug. 2013.

[11] I. M. Alsofyani and N. R. N. Idris, "Simple flux regulation for improving state estimation at very low and zero speed of a speed sensorless direct torque control of an induction motor," *IEEE Trans. Power. Electron.*, Vol. 31, No. 4, pp. 3027-3035, Apr. 2016.

[12] R. N. Andriamalala, H. Razik, J. N. Razafinjaka, L. Baghli, and F. Sargos,"Independent and direct rotor-flux oriented control of series-connected induction machines Using Decoupled Kalman-Filters," in *Proc. 37th Annual IEEE Conf. Ind. Electron. Soc.*, Melbourne, Australia, 2011, pp. 3488-3494.

[13] Y. C. Shi, K. Sun, L. P. Huang, and Y. D. Li, "Online identification of permanent magnet fluxbased on extended Kalman filter for IPMSM drive with position sensorless control," *IEEE Trans. Ind. Electron.*, Vol. 59, No. 11, pp. 4169-4178, Nov. 2012.

[14] L. Idkhajine, E. Monmasson, and A. Maalouf, "Fully FPGA-based sensorless control for synchronous AC drive using an extended Kalman filter," *IEEE Trans. Ind. Electron.*, Vol. 59, No. 10, pp. 3908-3918, Oct. 2012.

[15] A. Masi, M. Butcher, M. Martinoand, and R. Picatoste, "An application of the extended Kalman filter for a sensorless stepper motor drive working with long cables," *IEEE Trans. Ind. Electron.*, Vol. 59, No. 11, pp. 4217-4225, Nov. 2012.

[16] M. Bendjedia, Y. Ait-Amirat, B. Walther, and A. Berthon, "Position control of a sensorless stepper motor," *IEEE Trans. Power Electron.*, Vol. 27, No. 2, pp. 578-587, Feb. 2012.

[17] Z. G. Yin, C. Zhao, J. Liu, and Y. R. Zhong, "Research on anti-error performance of speed and flux estimator for induction motor using robust reduced-order EKF," *IEEE Trans. Ind. Informatics.*, Vol. 9, No. 2, pp. 1037-1046, May. 2013.

[18] N. K. Quang, N. T. Hieu, and Q. P. Ha, "FPGA-based sensorless PMSM speed control using reduced-order extended Kalman filters," *IEEE Trans. Ind. Electron.*, Vol. 61, No. 2, pp. 6574-6582, Dec. 2014.

[19] M. Habibullah and D. D. C. Lu, "A speed-sensorless FS-PTC of induction motors using extended Kalman filters," *IEEE Trans. Ind. Electron.*, Vol. 62, No. 11, pp. 6765-6778, Nov. 2015.

[20] N. Salvatore, A. Caponio, F. Neri, S. Stasi, and G. L. Cascella, "Optimization of delayed-state kalman-filter-based optimization of delayed-state Kalman-filter-based control of induction motors," *IEEE Trans. Ind. Electron.*, Vol. 57, No. 1, pp. 385-394, Jan. 2010.

[21] T. Schuhmann and W. Hofmann, "Improving operational performance of active magnetic bearings using Kalman filter and state feedback control," *IEEE Trans. Ind. Electron.*, Vol. 59, No. 2, pp. 821-829, Feb. 2012.

[22] M. Barut, R. Demir, E. Zerdali, and R. Inan, "Real-time implementation of bi input-extended Kalman filter-based estimator for speed-sensorless control of induction motors," *IEEE Trans. Ind. Electron.*, Vol. 59, No. 11, pp. 4197-4206, Nov. 2012.

[23] X. Xiao and C. Chen, "Dynamic permanent magnet flux estimation of permanent magnet synchronous machines," *IEEE Trans. Appl. Supercond.*,Vol. 20, No. 3, pp. 1085-1088, Jun. 2010.

[24] Z. G. Yin, C. Zhao, Y. R. Zhong, and J. Liu, "Research on robust performance of speed-sensorless vector control for the induction motor using an interfacing multiple-model extended Kalman filter," *IEEE Trans. Power. Electron.*, Vol. 29, No. 6, pp. 3011-3019, Jun. 2014.

[25] F. Alonge, T. Cangemi, F. D'Ippolito, A. Fagiolini, and A. Sferlazza, "Robustness analysis of an extended Kalman filter for sensorless control of induction motors," *IEEE Trans. Ind. Electron.*, Vol. 62, No. 4, pp. 2341-2352, Apr. 2015.

[26] K. Szabat, T. Orlowska-Kowalska, and M. Dybkowski, "Indirect adaptive control of induction motor drive system with an elastic coupling," *IEEE Trans. Ind. Electron.*, Vol. 56, No. 10, pp. 4038-4042, Oct. 2009.

[27] M. Hilairet, F. Auger, and E. Berthelot, "Speed and rotor flux estimation of induction machines using a two-stage extended Kalman filter," *Automatica*, Vol. 45, No. 8, pp. 1819-1827, Aug. 2009.

[28] V. Smidl and Z. Peroutka, "Advantages of square-root extended Kalman filter for sensorless control of AC drives," *IEEE Trans. Ind. Electron.*, Vol. 59, No. 11, pp. 4189-4196, Nov. 2012.

[29] G. H. B. Foo, X. A Zhang, and D. M. Vilathgamuwa, "A sensor fault detection and isolation method in interior permanent-magnet synchronous motor drives based on an extended Kalman filter," *IEEE Trans. Ind. Electron.*, Vol. 60, No. 8, pp. 3485-3495, Aug. 2013.

Zhonggang Yin was born in Shandong, China, in 1982. He received his B.S., M.S., and Ph.D. degrees in Electrical Engineering from the Xi'an University of Technology, Xi'an, China, in 2003, 2006 and 2009, respectively. In 2009, he joined the Department of Electrical Engineering, Xi'an University of Technology, where he is presently working as an Associate Professor. His current research interests include the high-performance control of ac motors, and the digital control of power converters.

Guoyin Li was born in Chongqing, China, in 1992. He received his B.S. degree in Electrical Engineering from the Xi'an University of Technology, Xi'an, China, in 2014. He is presently working towards his M.S. degree in Power Electronics and Electrical Drives in the Department of Electrical Engineering, Xi'an University of Technology. His current research interests include the high-performance control of ac motors.

Chao Du was born in Shaanxi, China, in 1991. He received his B.S. and M.S. degrees in Electrical Engineering from the Xi'an University of Technology, Xi'an, China, in 2013 and 2016, respectively. He is presently working towards his Ph.D. degree in Electrical Engineering at the Xi'an University of Technology. His current research interests include high performance ac drive systems and the optimization of their efficiency and parameters.

Xiangdong Sun was born in Shenyang, China, in 1971. He received his Ph.D. degree in Electrical Engineering from the Xi'an University of Technology, Xi'an, China, in 2003. He did Postdoctoral Research at the Tokyo Polytechnic University, Tokyo, Japan, supported by a government scholarship of Japan from 2006 to 2008. He is presently working as a Professor in the Department of Electrical Engineering, Xi'an University of Technology. His current research interests include motor control, power electronics, and renewable energy systems.

Jing Liu was born in Anhui, China, in 1982. She received her B.S., M.S., and Ph.D. degrees in Electrical Engineering from the Xi'an University of Technology, Xi'an, China, in 2003, 2006 and 2009, respectively. In 2009, she joined the Department of Electrical Engineering, Xi'an University of Technology, where she is presently working as an Associate Professor. Her current research interests include power semiconductor devices and their application to power electronic devices.

Yanru Zhong was born in Xi'an, China, in 1950. He received his B.S. degree in Electrical Engineering from the Xi'an Jiaotong University, Xi'an, China, in 1975; and his M.S. degree in Electrical Engineering from the Xi'an University of Technology, Xi'an, China, in 1983. He joined the faculty of the Xi'an University of Technology in 1983. He was a Visiting Scholar in the Department of Electrical Engineering of Sophia University, Tokyo, Japan, in 1987. Since 1993, he has been a Professor at the Xi'an University of Technology. His current research interests include power electronics, especially inverter and AC drive systems.